Acta Cryst. (1990). A46, 153-165

Physical and Mathematical Foundations of Multiwave Electron Diffraction

BY F. N. CHUKHOVSKII AND V. L. VERGASOV

Institute of Crystallography, Academy of Sciences of the USSR, 117333 Moscow, USSR

(*Received* 11 *November* 1988; *accepted* 16 *June* 1989)

Dedicated to the memory of Professor Z. G. Pinsker

Abstract

The dynamical problem of multiwave electron diffraction in perfect and imperfect crystals is treated on the basis of the Bloch wave formalism. In the case of a perfect crystal the classification of the electron Bloch states in terms of the transverse energy is introduced. A perturbation theory for the analytical construction of electron Bloch functions is suggested, using the symmetry of the dynamical matrix. The contribution of bound, valence and free Bloch states to the reflections and to high-resolution electron-microscopy (HREM) images are analysed. Using the column approximation, the equations describing the propagation and the excitation of the electron Bloch waves due to defects in a crystal lattice are derived from the Schrödinger equation. A solution of these equations is obtained in the first Born approximation. The theoretical foundation of the Cowley–Moodie multislice method for computer simulations of HREM images is presented. As an illustration of the Cowley–Moodie method, HREM images of Au in the ⟨110⟩ orientation and $Y_3Al_5O_{12}$ ⟨111⟩ are calculated for different defocusing parameters Δf. In the case of Au the fine structure of Au lattice images, when the Au atom strings are surrounded by 'halos', is clearly revealed for certain values of Δf. The Y–Al garnet images are shown to have either a sixfold or a threefold axis of symmetry, depending whether or not the dimensionless thickness in terms of the lattice spacing along ⟨111⟩ is an integer number.

1. Introduction

Amongst the numerous formulations of multiwave dynamical theory for fast electron diffraction three approaches are most widely known. Bethe (1928) elaborated the original approach based on the physical concept of Bloch waves propagating inside a crystalline medium. Another method similar to Darwin's for the treatment of reflection of X-rays from planes perpendicular to the crystal surface is developed by Howie & Whelan (1961). They give a mathematically rigorous justification of Darwin's method and derive a set of coupled first-order differential equations linking the diffracted-wave amplitudes in imperfect crystals. The third approach, which opened the way to computer simulations of high-resolution electron-microscopy (HREM) lattice images, was suggested by Cowley & Moodie (1959). It is based on a quasi-classical (electron-optical) approximation of quantum-mechanical theory.

The present paper deals with the general problem of dynamical electron diffraction based on the Bloch wave method. Special attention is paid to the electron energy classification of the transverse motion states (§2) and to the role of symmetry properties of the Bloch waves from the point of view of group theory (§3). In §4 the perturbation theory for the construction of many-beam Bloch wave functions is developed and in §5 the practical possibilities of the theory are discussed and illustrated by some examples. In §6 the problem of the Bloch wave scattering in a crystal with an arbitrary point defect is treated. In the framework of the column approximation the solution of the dynamical equations describing the Bloch wave excitation is obtained using first-order perturbation theory. In §7 the Cowley–Moodie multislice method for computer simulations of HREM images is briefly discussed and the results of numerical calculations for an Au lattice in the ⟨110⟩ orientation and a $Y_3Al_5O_{12}$ lattice ⟨111⟩ are presented and a qualitative analysis of the HREM image contrast variation is presented.

2. Transverse-energy classification of the electron Bloch states

In the general case the wave function $\psi(\mathbf{r})$ describing the propagation of an electron inside a medium obeys the relativistic Dirac equation. For non-magnetic crystals and fast electrons when the electron potential energy $U(\mathbf{r})$ is small in comparison with its total energy $\varepsilon = E + mc^2$, the Dirac equation can be transformed to the non-relativistic Schrödinger equation:

$$\Delta\psi(r) + 4\pi^2[K_0^2 + V(\mathbf{r})]\psi(\mathbf{r}) = 0, \qquad (1)$$

0108-7673/90/030153-13$03.00

where $K_0^2 = 2mh^{-2}E(1 + E/2mc^2)$, $V(\mathbf{r}) = -2mh^{-2}U(\mathbf{r})\,(1 + E/mc^2)$. Here, E, m are the kinetic energy and the rest mass of the electron, respectively, c is velocity of light, and h is Planck's constant.

The three-dimensional periodicity of the function $V(\mathbf{r})$ enables us to write the solution of (1) in the form of a Bloch wave

$$\psi(\mathbf{k}_0,\mathbf{r}) = \sum_g \psi_g(\mathbf{k}_0)\exp[i\,\pi(\mathbf{k}_0 + \mathbf{g}).\mathbf{r}], \qquad (2)$$

i.e. the scattered beams propagate discretely in the directions of the nodes $\{\mathbf{g}\}$ of the reciprocal lattice.

By substituting (2) into (1), we obtain (Hirsch, Howie, Nicholson, Pashley & Whelan, 1965) a set of linear homogeneous equations, which can be written in the form of the eigenvalue matrix equation

$$M\downarrow^j = x^j\psi^j, \quad j = 1, 2, \ldots, N. \qquad (3)$$

Here ψ^j is the jth eigenvector

$$\psi^j \equiv \psi(\mathbf{k}_0^j) = \begin{Vmatrix} \psi_0^j \\ \psi_h^j \\ \psi_g^j \\ \vdots \end{Vmatrix} \qquad (4)$$

and

$$x^j \simeq 2K_z(k_{0z}^j - K_z) \qquad (5)$$

is the jth eigenvalue of the dynamical matrix M,

$$M = \begin{Vmatrix} 0 & V_{0h} & V_{0g} & \cdots \\ V_{h0} & D_h & V_{hg} & \cdots \\ V_{g0} & V_{gh} & D_g & \\ \vdots & \vdots & & \ddots \end{Vmatrix}, \qquad (6)$$

where $V_{gh} = \Omega^{-1}\int V(\mathbf{r})\exp[-i2\pi(\mathbf{g} - \mathbf{h})\mathbf{r}]\mathrm{d}\mathbf{r}$, $D_h = \mathbf{K}^2 - (\mathbf{K} + \mathbf{h})^2$, $K^2 = K_0^2 + V_0$, $V_0 \equiv V_{hh}$, z denotes the thickness of the crystalline slab, and Ω is the volume of the unit cell. The diagonal elements D_h can be rewritten in terms of the distance s_h (excitation error) of the node h from the Ewald sphere as follows: $D_h = 2K_2s_h$.

Thus the wave vectors of electrons in a crystal turn out to be quantized:

$$\mathbf{k}_0^j = (k_{0z}^j, \mathbf{k}_{0\rho}^j) \simeq (K_z + x^j/2K_z, \mathbf{K}_\rho), \qquad (7)$$

and the wave function $\psi(\mathbf{r})$ is a linear combination of N Bloch waves:

$$\psi(\mathbf{r}) = \sum_{j=1}^{N} \alpha^j\psi^j(\mathbf{r}) \equiv \sum_{j=1}^{N} \alpha^j\psi(\mathbf{k}_0^j, \mathbf{r}). \qquad (8)$$

Here α^j is the excitation amplitude of the jth Bloch wave; $\varepsilon^j \equiv |\alpha^j|^2$ is the population of the jth quantum electron state and, hence, obeys the equality

$$\sum_{j=1}^{N} \varepsilon^j = 1.$$

Physically, this means that the parameter ε^j is the probability of finding the electron in the jth Bloch state. In the case of a non-absorbing crystal $\alpha^j = \psi_0^{j*}$. Then the wave function (8) can be represented by

$$\psi(\mathbf{r}) = \sum_{j=1}^{N} \psi_h(z)\exp[i2\pi(\mathbf{K} + \mathbf{h}).\mathbf{r}], \qquad (9)$$

where the hth diffracted-beam amplitude takes the form

$$\psi_h(z) = \sum_{j=1}^{N} \omega_h^j\exp(i\pi x^j\mathbf{z}/K_z); \qquad (10)$$

in other words, all Bloch waves excited in the crystal participate in the formation of each reflection of the electron diffraction pattern, and the quantity $\omega_h^j = \alpha^j\psi_h^j$ is the excitation amplitude of the jth Bloch wave in the hth reflection.

In the case of fast electron diffraction the inequality $|V_{0h}/D_h| \gtrsim 1$ takes place for a very large number N_0 of nodes. This means that at least N_0 eigenvalues of the matrix M depend strongly on the off-diagonal elements, whereas another $N - N_0$ eigenvalues can be determined with good accuracy by the diagonal elements of the matrix M only. Thus the eigenvalue problem (3)–(6) reduces to the solution of the dispersion equation of N_0th order ($N_0 \gg 1$) at least; and that is what the well known problem of multiwave electron diffraction amounts to. Generally, multiwave diffraction is connected with the geometrical fact that many nodes are in a position close to the Bragg position $|\mathbf{K}| = |\mathbf{K} + \mathbf{h}|$, because the magnitudes of the reciprocal-lattice vectors involved are small in comparison with the radius K of the Ewald sphere (for $E = 100$ keV, $h/K \sim 10^{-2}$). It is clear that the Bragg condition will be satisfied best for the vectors $\{\mathbf{h}\}$ of the reciprocal-lattice plane perpendicular to the incident wave vector $\mathbf{K}$. Taking into account the nodes of the reference plane only (the so-called zeroth-order Laue plane, $\mathbf{h}_z = 0$) is evidently adequate for the averaging of the crystal potential $V(\mathbf{r})$ over the z direction,

$$\mathrm{V}(\mathbf{r}) \rightarrow V(\boldsymbol{\rho}) = \sum_h V_{\mathbf{h}}\exp(i2\pi\mathbf{h}.\boldsymbol{\rho}).$$

Physically this means that the fast electrons moving along the crystallographic axes or planes are not 'sensitive' to the variations of $V(\mathbf{r})$ in the direction of their motion. Such constant potentials along the z axis of atomic strings or planes are typical in theories of axial and planar channeling, respectively (Vorobiev, 1984; Kalashnikov, Remizovich & Ryazanov, 1980). The latter type of motion corresponds to the well known case of systematic reflections in diffraction theory.

Thus the use of the two-dimensional crystal potential $V(\boldsymbol{\rho})$ (one-dimensional in the case of planar

channeling) has the result that the original three-dimensional quantum-mechanical problem becomes two-dimensional (one-dimensional). Otherwise, the electron Bloch waves are quantized in the plane transverse to the incident wave vector in such a way that one of the main characteristics of the Bloch states is the transverse energy

$$E_\perp^j = \mathbf{K}_0^2 - (k_{0z}^j)^2 \simeq -(x^j + V_0 - K_\rho^2). \qquad (11)$$

According to $E_\perp^j$ values, the Bloch waves are divided into sub-barrier ($E_\perp^j \ll -V_0$), near-barrier ($|E_\perp^j| \sim |V_0|$) and above-barrier waves ($E_\perp^j \gg V_0$) and the corresponding electron states are determined as the bound, valence and free states.

3. Symmetry classification of the Bloch states; reduction of the dynamical matrix

Generally, in order to find the multiwave Bloch states, computer calculations are needed because the dynamical matrix $M(6)$ is of rank N. Nevertheless, in some cases of practical interest the problem can be solved analytically. Indeed, the dynamical matrix contains information about the crystal symmetry and the boundary conditions in its off-diagonal and diagonal elements, respectively. So, for certain directions of the incident beam, in particular, along the crystallographic axes or when a set of nodes lies on the Ewald sphere, the matrix M in the zeroth-order Laue-zone approximation acquires the symmetry of one of the nine plane crystallographic groups. In such cases the totality of nodes in the zeroth-order Laue zone can be represented as a set of stars, each of them consisting of nodes which have the same excitation errors s_h and which are connected with equal Fourier components $V_\mathbf{h}$ of the potential. As an example, in Fig. 1 such stars numbered 1 to 9 are shown for a ⟨100⟩ LiF crystal with the 200 node lying on the Ewald sphere.

In cases in which the matrix M possesses the symmetry group R, its rank can be effectively reduced by making use of the group-theoretical classification of the electron Bloch states. If the operators $\{r\}$ are elements of the symmetry group $R(r_1, r_2, \ldots, r_H)$ of the N-rank matrix M, then the N-rank matrix representation $D(r)$ for an arbitrary r from R will commute with the dynamical matrix M since the symmetry is the integral of motion. In the general case the representation $D(r)$ is reducible, *i.e.* the matrix $D(r)$ can be brought to the block-diagonal form

$$\bar{D}(r) \equiv T^{-1}D(r)T = \left\| \begin{array}{ccccccc} D^{(p)}(r) & 0 & \ldots & 0 & 0 & \ldots \\ 0 & D^{(p)}(r) & & & & \\ \vdots & & \ddots & & & \\ 0 & & & D^{(p)}(r) & 0 & \ldots \\ 0 & & & 0 & D^{(p')}(r) & \\ \vdots & & & & & \ddots \end{array} \right\|$$

$$\equiv \sum_p \oplus n(p) D^{(p)}(r). \qquad (12)$$

In (12) each block $D^{(p)}(r)$ is the pth irreducible representation of the element r and occurs $n(p)$ times in the reducible representation. This is written using the symbol $\oplus$ for the direct sum. Each matrix $D^{(p)}(r)$ has the rank $i(p)$ equal to the dimension of the irreducible representation $D^{(p)}(r)$; for the plane point groups considered here, $i(p) \leq 2$.

Since the dynamical matrix M commutes with the matrix $D(r)$ reducible to the block-diagonal form, it can also be reduced according to Wigner's theorem (Streitwolf, 1967) to the block-diagonal form using the same matrix T. It is easy to see that the N-row columns $\varphi_\mu^{(p),n}$, $\mu = 1, 2, \ldots, i(p)$, $n = 1, 2, \ldots, n(p)$, which satisfy the equality

$$r\varphi_\nu^{(p),n} = \sum_{\nu=1}^{i(p)} \varphi_\nu^{(p),n} D_{\nu\mu}^{(p)}(r) \qquad (13)$$

and which are called the basis functions of the μth row of the pth representation, are the columns of the matrix T. The basis functions $\varphi_\mu^{(p),n}$ are constructed (Kogiso & Takahashi, 1977) using the nilpotent projection operators

$$\rho_{\mu\nu}^{(p)} = H^{-1}(R) i(p) \sum_{r=1}^{H(R)} D_{\mu\nu}^{(p)*}(r) r, \qquad (14)$$

which operate on an arbitrary function φ of the N-dimensional space of the N-row columns to give the basis function of the μ row of the irreducible representation $D^{(p)}(r)$. The functions $\{\varphi_\mu^{(p),n}\}$ constructed in this manner are orthogonal with respect to the indices p and rows μ of the representations $D^{(p)}(r)$ and in the general case are not orthogonal with respect to the indices n of their multiplicity. To overcome this inconvenience and, hence, to make the reduction matrix T unitary, we use the following technique (Vergasov & Chukhovskii, 1983).

Consider, first, a separate kth star of the general form, *i.e.* such that the number N_k of its nodes is equal to the order of the group $H(R)$, $N_k = H(R)$. The reducible representation D_k corresponding to

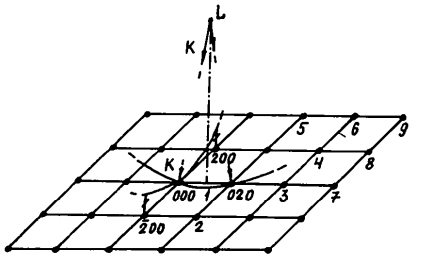

Fig. 1. The zeroth-order Laue plane (100) of an LiF crystal. The 020 node is in the exact Bragg position. The symmetry group is C_{2v}. The stars numbered include nodes: 1 (000, 020), 2 ($\bar{2}20$, 220, 200, $\bar{2}00$), 3 (040, $0\bar{2}0$), 4 (240, $2\bar{2}0$, $\bar{2}\bar{2}0$, $\bar{2}40$), 5 (420, 400, $\bar{4}00$, $\bar{4}20$), 6 (440, $4\bar{2}0$, $\bar{4}\bar{2}0$, $\bar{4}40$), 7 (060, $0\bar{4}0$), 8 (260, $2\bar{4}0$, $\bar{2}\bar{4}0$, $\bar{2}60$), 9 (460, $4\bar{4}0$, $\bar{4}\bar{4}0$, $\bar{4}60$).

this star is regular, $D_k = D_R$, and the multiplicity of each $D^{(p)}$ in D_k equals the dimension of $D^{(p)}$, $n(p, k \equiv R) = i(p)$. Then the orthonormal set of the basis functions $\varphi_\mu^{(p),n}$ corresponding to this star can be obtained by applying the operators $\rho_{\mu\nu}^{(p)}$ (14) to an arbitrary N_k-row column; the index ν is identified with the index $n(p, k \equiv R)$ (Landau & Lifshits, 1974). If the kth star is a star of the special form, when $N_k < H(R)$, the problem is solved by excluding the linearly dependent functions from the set of functions $\{\varphi_{\mu,k}^{(p),\nu}\}$ obtained at every fixed μ, and, next, by orthonormalizing the remaining functions. Consider now the construction of basis functions for the assembly of N nodes consisting of l stars $N = \sum_{k=1}^{l} N_k$. By the definition of the star the projection operator (14) does not mix the components of the N-row column corresponding to different stars and, therefore, the whole space of these columns can be represented as a direct sum of subspaces of the N_k-row columns. Then, the natural choice for the orthonormal set of basis functions is

$$\begin{aligned}\varphi_\mu^{(p),1} &= \sum_{k=1}^{l} \oplus \varphi_{\mu,k}^{(p),1}\,\delta_{k1}, \ldots, \varphi_\mu^{(p)n(p,1)} \\ &= \sum_{k=1}^{l} \oplus \varphi_{\mu,k}^{(p),n(p,k)}\,\delta_{k1}, \\ \varphi_\mu^{(p),n(p,1)+1} &= \sum_{k=1}^{l} \oplus \varphi_{\mu,k}^{(p),1}\,\delta_{k2}, \ldots, \varphi_\mu^{(p),n(p)} \\ &= \sum_{k=1}^{l} \oplus \varphi_{\mu,k}^{(p),n(p,k)}\,\delta_{kl}. \end{aligned} \tag{15}$$

It is essential that the explicit form of the reduced matrix $\overline{M} = T^{-1}MT$ depends on the arrangement of the basic functions $\varphi_\mu^{(p),n}$ in the reduction matrix T. For example, if we choose T in the form

$$\begin{aligned} T &= \|T_1^{(p)} T_2^{(p)} \ldots T_{i(p)}^{(p)} T_1^{(p')} \ldots\|, \\ T^{(p)} &= \|\varphi_\mu^{(p),1}\, \varphi_\mu^{(p),2} \ldots \varphi_\mu^{(p),n(p)}\|, \end{aligned} \tag{16}$$

it will give the dynamical matrix M in the following block-diagonal form (Kogiso & Takahashi, 1977)

$$T^{-1}MT = \overline{M} = \sum_p \oplus i(p) M^{(p)}, \tag{17}$$

where

$$M^{(p)} = \begin{Vmatrix} M_{11}^{(p)} & \ldots & M_{1n(p)}^{(p)} \\ \vdots & & \vdots \\ M_{n(p)1}^{(p)} & \ldots & M_{n(p)n(p)}^{(p)} \end{Vmatrix}. \tag{18}$$

Then (3) will be transformed to

$$\overline{M}\,\overline{\psi}^j = x^j \overline{\psi}^j, \quad j = 1, 2, \ldots, N, \tag{19}$$

where $\overline{\psi}^j = T^{-1}\psi^j$.

In view of (17), (19) will be broken into the set of equations

$$M^{(p)} \overline{\psi}^{j(p)} x^{j(p)} \overline{\psi}^{j(p)}, \quad j = 1, 2, \ldots, n(p). \tag{20}$$

It is clear that

$$\{\overline{\psi}^j\} = \left\{ \sum_p \oplus \overline{\psi}^j(p) \right\}, \quad N = \sum_p n(p).$$

Thus, to each irreducible representation $D^{(p)}$ there correspond $n(p)$ different Bloch states, any of which is $i(p)$-fold degenerate. This means that the electron Bloch states $\psi^j(r)$ are classified not only by their dependence on the magnitude of the transverse energy $E^j_\perp$ but also according to the irreducible representations $D^{(p)}$ and their rows μ: $j \to j(p, \mu)$.

An important point of the reduction procedure of the dynamical matrix M possessing the symmetry group R is how to determine for any system of stars the highest number $n_0 \doteq \max_p\{n(p)\}$. This in turn coincides with the highest order of the dispersion equations each of which corresponds to the irreducible representation $D^{(p)}$. This could be done by means of the formulae obtained by Kogiso & Takahashi (1977) for $n(p)$ for all plane symmetry groups. However, the problem can be solved by the simple method proposed previously (Vergasov, Chukhovskii & Pinsker, 1982). Using the characteristic properties of the stars it was proved that

$$n_0 = \begin{cases} l & \text{for groups } C_s,\ C_n,\ C_{2v} \\ \max\{l, l' + l_g\} & \text{for groups } C_{nv},\ n = 3, 4, 6. \end{cases}$$

Here l and l' are the total number of stars with and without the central node, respectively; l_g is the number of stars of the general form.

In the cases of interest, especially in high-resolution electron microscopy, the electron beam falls normally onto a crystal. The following statement will be true here. The Bloch waves of the unitary irreducible representation only are excited at normal incidence, and the number of these waves is equal to the number l of the stars involved. The jth Bloch wave excitation amplitude α^j is determined by the component ψ_0^{j*} corresponding to the incident beam. At normal incidence the corresponding node 000 is central in the electron diffraction pattern and does not change its position under the action of the operators $\rho_{\mu\nu}^{(p)}$ of the symmetry group R. Then, using the formalism of the operators, we obtain

$$\psi_0^{j(p)} \sim \rho_{\mu\nu}^{(p)} 1 \sim \sum_r D_{\mu\nu}^{(p)*}(r) \sim \delta_{pu} \tag{21}$$

in accordance with the orthogonality relations for irreducible representations (Streitwolf, 1967). Further, since the unitary representation $D^{(u)}(r) = 1$ is one-dimensional, *i.e.* $i(u) = 1$, the reducible representation D_k describing each kth star contains the unitary representation $D^{(u)}$ only once, $n(u, k) = 1$. Hence, the number of Bloch waves in the unitary representation is equal to the total number of stars

involved,

$$n(u) = \sum_{k=1}^{l} n(u, k) = l.$$

The above result permits us to restrict our consideration of (20), in this case, only to the block of unitary representations $M^{(u)} = (T^{(u)})^{-1} M T^{(u)}$. It is essential that we can obtain the general expression for $M^{(u)}$ since the structure of unitary representations does not depend on the type of the group R. The basis function corresponding to the kth star takes the form $\varphi^{(u)}_{1,k}{}^{1+} = N_k^{-1/2}(11...1)$ so that

$$(T^{(u)})^{-1} = \begin{Vmatrix} 1 & 0 & \dots & & & \\ 0 & N_2^{-1/2} & \dots & N_2^{-1/2} & 0 & \dots \\ 0 & \dots & 0 & N_3^{-1/2} & \dots & N_3^{-1/2}\ 0 \dots \\ \vdots & & & & & \end{Vmatrix}$$

and the matrix $T^{(u)}$ is obtained from $(T^{(u)})^{-1}$ by interchanging rows and columns.

Denoting the hth node of the kth star with the index k, $h \equiv h(k)$, and bearing in mind the fact that at the normal incidence $D_{g(k)} = -g^2(k)$, we write the matrix M in the form

$$M = \begin{Vmatrix} 0 & V_{0(1)g(2)} & V_{0(1)g'(2)} & \dots & V_{0(1)h(3)} & \dots \\ V_{g(2)0(1)} & -g^2(2) & V_{g(2)g'(2)} & \dots & V_{g(2)h(3)} & \dots \\ V_{g'(2)0(1)} & V_{g'(2)g(2)} & -g'^2(2) & \dots & V_{g'(2)h(3)} & \dots \\ \vdots & \vdots & \vdots & \ddots & & \\ V_{h(3)0(1)} & V_{h(3)g(2)} & V_{h(3)g'(2)} & \dots & -h^2(3) & \\ \vdots & \vdots & \vdots & & & \ddots \end{Vmatrix}.$$

Taking into account the relations $V_{0(1)g(2)} = V_{0(1)g'(2)} = \dots$ and

$$\sum_{h=1}^{N_k} \sum_{g=1}^{N_g} M_{h(k)g(s)} = N_k \sum_{g=1}^{N_s} M_{h(k)g(s)} = N_s \sum_{h=1}^{N_k} M_{h(k)g(s)},$$

we find the block $M^{(u)}$ finally

$$M^{(u)} = \begin{Vmatrix} 0 & N_2^{1/2}V_{0(1)g(2)} & N_3^{1/2}V_{0(1)h(3)} & \dots \\ N_2^{1/2}V_{g(2)0(1)} & D^{(u)}_{g(2)} & (N_3N_2^{-1})^{1/2}\sum_g V_{g(2)h(3)} & \dots \\ N_3^{1/2}V_{h(3)0(1)} & (N_3N_2^{-1})^{1/2}\sum_g V_{h(3)g(2)} & D^{(u)}_{h(3)} & \\ \vdots & & & \ddots \end{Vmatrix} \quad (22)$$

where

$$D^{(u)}_{g(k)} = -g^2(k) + \sum_g{}' V_{g(k)h(k)} \quad (23)$$

and the symbol $\sum'_g$ denotes, as usual, the summation over all indices $g(k)$ except for $g(k) = h(k)$.

A different classification of the electron states in crystals is suggested in the framework of channeling theory (Kambe, Fujimoto & Lehmpfuhl, 1974). If the levels of the bound states $E^j_\perp \ll -V_0$ in the potential well of the atomic plane or axis are sufficiently low-lying, these states are not affected by the potentials of the neighboring planes or axes. For this reason, in channeling theory, the approximation of an isolated plane or axis potential is utilized, along with the notion of continuum potential for a plane or axis. For planar channeling, corresponding to a one-dimensional quantum-mechanical problem, the electron states can be classified as symmetric and antisymmetric (Landau & Lifshits, 1974). For axial channeling the radial part $R_{nl}(\rho)$ of the wave function $\psi(\mathbf{r})$

$$\sum_{n,l} \alpha^{nl} R_{nl}(\rho) \exp(il\varphi)$$

satisfies the equation

$$R''_{nl}(\rho) + \rho^{-1}R'_{nl}(\rho) - l^2\rho^{-2}R_{nl}(\rho) = [V(\rho) - E^{nl}_\perp]R_{nl}(\rho).$$

This equation takes the same form as the one for the one-electron atom, so that the electron states are classified as *ns*, *np*, ... according to the azimuthal quantum numbers $l = 0$, $l = 1$, ..., respectively. It is clear that when the beam impinges strictly parallel to the atomic string, the only populated states in the crystal will be the *s* states with radial symmetry of density distribution. When the beam deflects from the crystallographic axis, the populated states will also be the states with $l \neq 0$ whose density distributions have no radial symmetry.

Now it is easy to establish the relationship between the quasi-atomic and group-theoretical classifications of the electron states. In the case of planar channeling, the diffraction pattern is a sequence of systematic reflections and has the symmetry C_s with two irreducible representations. The symmetric electron states correspond to the Bloch waves of the unitary representation. Likewise, for axial channeling, the *s* waves correspond to the states of the unitary representation, and the states with a non-zero orbital momentum correspond to non-unitary states including the two-dimensional ones.

It is to be noted, however, that the group-theoretical classification is more rigorous and general since it does not use the isolated axis (plane) approximation. In addition, dynamical theory describes equally well sub-, above- and near-barrier states. The latter, as will be seen from the following, plays a crucial role in the construction of the electron wave function in question.

4. Perturbation theory

The rank of the dynamical matrix is so high that, in spite of its reduction in order to construct an analytic solution to (3), it is necessary to use the perturbation method. For simplicity we consider the case of normal incidence, *i.e.* when only the Bloch waves of the unitary representation are excited and the block $M^{(u)}$ acts as an initial dynamical matrix. It is easy to see that the Bloch waves of other irreducible representations can be constructed in a similar way. Moreover, the perturbation method is also applicable to the original dynamical matrix $M(6)$ when it possesses the trivial symmetry group C_1.

Let us arrange the stars in block $M^{(u)}$ in descending order of the α parameter [see (22)]:

$$\alpha_{1k}^{(u)} = |N_k^{1/2} V_{0(1)g(k)}/D_{g(k)}^{(u)}| \qquad (24)$$

(for simplicity, here we consider $V_{0(1)g(k)} \neq 0$). The above parameter determines the strength of the interaction between the transmitted beam $0(1)$ and the N_k diffracted beams of the kth star; it could also be qualitatively interpreted as the amplitude of transition from the ground ($k = 1$) o th kth ($k \neq 1$) electron Bloch state.

If $\alpha_{1k}^{(u)} \geq 1$ for the stars $k = 2, 3, ..., I$ the eigenvalues $x^{1(u)}, x^{2(u)}, ..., x^{L(u)}$ of the matrix $M^{(u)}$ depend essentially on its corresponding off-diagonal elements and in the zeroth-order approximation the corresponding electron states should be found from the Lth-order dispersion equation

$$\det\|M_L^{(u)} - x_L^j E\| = 0, \quad j = 1, 2, ..., L, \qquad (25)$$

where $M_L^{(u)}$ is the L-rank matrix $M^{(u)}$ (22).

In other words, in this case the diffracted beams of the L stars are strongly interacting and must be considered simultaneously. If the number L is not large, we have in practice $|x_L^{j(u)}| \sim |V_{0(1)g(L)}|$ and the corresponding electron states with $E_\perp^{j(L,u)} = -(x_L^{j(u)} + V_0)$ are bound or valence states.

For the other systems $k = L+1, L+2, ...$ the parameter $\alpha_{1k}^{(u)} \ll 1$ and the eigenvalues of the matrix $M^{(u)}$ are determined in the zeroth-order approximation by its diagonal elements in such a way that the corresponding electron states with $E_\perp^{j(k,u)} \simeq g^2(k)$ are free states.

Thus, the zeroth-order $M^{(u)}$ matrix has the form

$${}_0M^{(u)} = \begin{Vmatrix} M_L^{(u)} & 0 & 0 & \cdots \\ 0 & D_{h(L+1)}^{(u)} & 0 & \cdots \\ 0 & 0 & D_{g(L+2)}^{(u)} & \\ \vdots & \vdots & & \ddots \end{Vmatrix} \qquad (26)$$

and the corresponding eigenvalues and eigenfunctions are determined as

$${}_0x^{j(L,u)} = x_L^{j(u)}, ..., {}_0x^{L+1(u)} = D_{h(L+1)}^{(u)}, ...$$

$${}_0\overline{\psi}^{j(L,u)} = \begin{Vmatrix} \overline{\psi}_L^{j(u)} \\ 0 \\ 0 \\ \vdots \end{Vmatrix}, ..., {}_0\overline{\psi}^{L+1(u)} = \begin{Vmatrix} 0 \\ 1 \\ 0 \\ \vdots \end{Vmatrix}, ... \qquad (27)$$

where the $\overline{\psi}_L^{j(u)}$ are the eigenfunctions of the matrix $M_L^{(u)}$

$$M_L^{(u)} \overline{\psi}_L^{j(u)} = x_L^{j(u)} \overline{\psi}_L^{j(u)}, \quad j = 1, 2, ..., L. \qquad (28)$$

The form of the solutions (27) permits us to draw an important conclusion: the Bloch waves, solutions of the Schrödinger equation, are determined by the complete set of stars of reciprocal-lattice vectors, but they are actually determined by a finite number of stars, and in the case of above-barrier waves each Bloch wave is largely determined by one such star.

For the non-relativistic electrons considered here, the transverse potential wells $V(\rho)$ contain no more than 1–2 bound states (*e.g.* Steeds, Jones, Cooke & Loveluck, 1977). Therefore, the total number of bound and valence states L is equal to or less than 3 as a rule. As a result, these and the free states can first be calculated analytically in the zeroth-order approximation and then with the desired accuracy by the perturbation method (Vergasov, Chukhovskii & Pinsker, 1984). Correspondingly, the perturbation is the matrix $U^{(u)} = M^{(u)} - {}_0M^{(u)}$ which describes the interaction of sub- and near-barrier waves with the above-barrier waves and also the interaction among the above-barrier waves themselves.

From the solutions in the zeroth-order approximation it is seen that the Bloch wave excitation amplitudes ${}_0\psi_0^{L+k*}$, $k = 1, 2, ...$ are equal to zero and, consequently, only L bound and valence states may be strongly populated in a crystal. Accordingly, the electron wave function $\psi^j(\mathbf{r})$ is for the most part determined by L sub- and near-barrier Bloch waves. Physically, this result is explained by the fact that most electrons populate states with the least transverse momentum.

It is to be noted that the conclusion about the predominant population of a few electron states was made by Komaki, Asano & Fujimoto (1977) on the basis of computations in the framework of channeling theory. The energy increase of the incident beam leads, apparently, to an increase in the number of levels in the potential well. In this case the perturbation method is not efficient. However, the increased number of bound states permits one to go over to a quasi-classical description of the diffraction phenomenon.

Let us now construct solutions of (20) using perturbation theory. We expand the unknown eigen-

function $\overline{\psi}^j$ in a series of eigenfunctions of zeroth-order approximation (for simplicity, we omit here the symbol of unitary representation)

$$\overline{\psi}^j = \sum_i C(j,i)\,{}_0\overline{\psi}^i. \tag{29}$$

Then, substituting (29) into (20) one obtains the equation

$$C(j,s)(x^j - {}_0x^s) = \sum_i C(j,i)U^{si}, \tag{30}$$

where

$$U^{si} = {}_0\overline{\psi}^{s+}\,U\,{}_0\overline{\psi}^i$$

and

$$U^{L+iL+s} = (N_s N_i^{-1})^{1/2}\sum_g V_{g(i)h(s)}.$$

The coefficients $C(j,s)$ and the eigenvalues x^j are expressed as series (Landau & Lifshits, 1974):

$$C(j,i) = \delta_{ji} + {}_1C(j,i) + {}_2C(j,i) + \ldots \tag{31}$$

$$x^j = {}_0x^j + {}_1x^j + {}_2x^j + \ldots, \tag{32}$$

where ${}_nC(j,i)$, ${}_nx^j$ are assumed to be of the same order as $(U)^n$.

Upon substitution of (31) and (32) into (30) we find the corresponding corrections by equating in (30) the terms of the same order. From the equation

$${}_1x^j\delta_{js} + {}_1C(j,s)({}_0x^j - {}_0x^s) = U^{sj} \tag{33}$$

which follows from (30) if only the first-order terms are retained, we obtain

$${}_1x^j = 0,\ {}_1C(j,j) = 0,\ {}_1C(j,s) = U^{sj}/({}_0x^j - {}_0x^s). \tag{34}$$

Thus, in first-order perturbation theory the solutions have the form

$${}_{0+1}\overline{\psi}^{j(L)} = \left\| \begin{matrix} \overline{\psi}^j_L \\ {}_1C(j,L+1) \\ {}_1C(j,L+2) \\ \vdots \end{matrix} \right\|, \ldots,$$

$${}_{0+1}\overline{\psi}^{L+1} = \left\| \begin{matrix} \sum_{j=1}^{L} {}_1C[L+1,j(L)]\overline{\psi}^j_L \\ 1 \\ {}_1C(L+1,L+2) \\ \vdots \end{matrix} \right\|. \tag{35}$$

It is easy to see that now the above-barrier Bloch waves are excited, which leads to the 'appearence' of the corresponding stars of reflections in the electron diffraction pattern.

Finally, we obtain the following expressions for the diffracted beam amplitudes:

$${}_{0+1}\psi_{h(k)} = {}_0\psi_{h(k)} = \sum_{j=1}^{L} \psi^{j*}_{0(1)}\psi^j_{h(k)} \exp(i\pi x^j_L K_z^{-1} z),$$

$$k = 1,2,\ldots,L; \tag{36}$$

$${}_{0+1}\psi_{h(L+n)} = \sum_{j=1}^{L} iN_{L+n}^{-1/2}\psi^{i*}_{0(1)}U^{L+nj(L)} \times \exp[i\pi 2^{-1}(x^j_L + x^{L+n})K_z^{-1}z] \times \sin[\pi 2^{-1}(x^j_L - x^{L+n})K_z^{-1}z] \times [2^{-1}(x^j_L - x^{L+n})]^{-1}, \quad n = 1,2,\ldots, \tag{37}$$

where the relation $\psi^j_{h(k)} = N_k^{-1/2}\overline{\psi}^j_{h(k)}$ has been taken into account.

The physical meaning of the first-order expressions (36), (37) is the following: the amplitudes of the diffracted beams belonging to L stars coincide with the zeroth-order values, whereas the expression (37) for the amplitudes of the beams of the other stars is like that given by kinematical theory. The only difference is that the role of the transmitted beam is played by the beams belonging to L stars.

In second-order perturbation theory (30) takes the form

$${}_2x^j\delta_{js} + {}_2C(j,s)({}_0x^j - {}_0x^s) = \sum_i {}_1C(j,i)U^{si}. \tag{38}$$

Using the normalization condition for the eigenfunctions, from (38) we obtain

$$\begin{aligned} {}_2C(j,s) &= \sum_i {}_1C(j,i)U^{si}/({}_0x^j - {}_0x^s), \\ {}_2C(j,j) &= -2^{-1}\sum_s |{}_1C(j,s)|^2, \\ {}_2x^j &= \sum_i {}_1C(j,i)U^{ji}. \end{aligned} \tag{39}$$

Hence, the second-order solutions are the following:

$${}_{0+1+2}\overline{\psi}^{j(L)} = \left\| \begin{matrix} \overline{\psi}^j_L + \sum_s^L {}_2C(j,s)\overline{\psi}^s_L \\ {}_{1+2}C(j,L+1) \\ {}_{1+2}C(j,L+2) \\ \vdots \end{matrix} \right\|, \ldots,$$

$${}_{0+1+2}\overline{\psi}^{L+1} = \left\| \begin{matrix} \sum_j^L {}_{1+2}C[L+1,j(L)]\overline{\psi}^j_L \\ {}_{1+2}C(L+1,L+1) \\ {}_{1+2}C(L+1,L+2) \\ \vdots \end{matrix} \right\| \tag{40}$$

Retaining the second-order terms, we finally obtain for the diffracted beam amplitudes

$${}_{0+1+2}\psi_{h(k)} = \sum_{j=1}^{L} {}_{0+1+2}\omega^{j(L)}_{h(k)} \exp(i\pi_{0+2}x^j_L K_z^{-1} z) + \sum_n {}_{0+1+2}\omega^{L+n}_{h(k)} \exp(i\pi_{0+2}x^{L+n}K_z^{-1}z), \tag{41}$$

$$
{}_{0+1+2}\psi_{h(L+n)} = \sum_{j=1}^{L} {}_{0+1+2}\omega^{j(L)}_{h(L+n)} \exp(i\pi_{0+2} x^{j}_{L} K_z^{-1} z)
$$

$$
+ {}_{0+1+2}\omega^{L+n}_{h(L+n)} \exp(i\pi_{0+2} x^{L+n} K_z^{-1} z)
$$

$$
+ \sum_{s \neq n} {}_{0+1+2}\omega^{L+s}_{h(L+n)}
$$

$$
\times \exp(i\pi_{0+2} x^{L+s} K_z^{-1} z), \qquad (42)
$$

where

$$
{}_{0+1+2}\omega^{j(L)}_{h(k)} = \psi^{j(L)*}_{0(1)} \psi^{j(L)}_{h(k)} + \sum_{s=1}^{L} \psi^{j(L)*}_{0(1)} \psi^{s(L)}_{h(k)2} C[j(L), s(L)]
$$

$$
+ \sum_{s=1}^{L} \psi^{s(L)*}_{0(1)} \psi^{j(L)}_{h(k)2} C^*[j(L), s(L)], \qquad (43)
$$

$$
{}_{0+1+2}\omega^{L+n}_{h(k)} = \sum_{s,j=1}^{L} \psi^{s(L)*}_{0(1)} \psi^{j(L)}_{h(k)1} C^*[L+n, s(L)]
$$

$$
\times {}_{1}C[(L+n, j(L)] N^{-1/2}_{L+n}, \qquad (44)
$$

$$
{}_{0+1+2}\omega^{j(L)}_{h(L+n)} = \psi^{j(L)*}_{0(1)} {}_{1+2}C[j(L), L+n] N^{-1/2}_{L+n}, \qquad (45)
$$

$$
{}_{0+1+2}\omega^{L+n}_{h(L+n)} = \sum_{j=1}^{L} \psi^{j(L)*}_{0(1)} {}_{1+2}C^*[L+n, j(L)] N^{-1/2}_{L+n}, \qquad (46)
$$

$$
{}_{0+1+2}\omega^{L+s}_{h(L+n)} = \sum_{j=1}^{L} \psi^{j(L)*}_{0(1)} {}_{1}C^*[L+s, j(L)]
$$

$$
\times {}_{1}C(L+s, L+n) N^{-1/2}_{l+n}, \qquad (47)
$$

where $k = 1, 2, ..., L$, $n = 1, 2, ..., s \neq n$.

It is worth noting that the expressions obtained above are valid if the inequality

$$
|{}_{1}C(i, j)| \ll 1 \qquad (48)
$$

holds.

5. Electron Bloch waves for calculating diffracted beam intensities and crystal lattice images

From the expressions (40)–(47) it follows that all reflections of the electron diffraction pattern can be divided into two groups. The first group is all reflections belonging to L stars which contain the major part of the intensity of the incident beam. It is easy to see from (41), (42) that the sub- and near-barrier waves contribute mainly to the intensities $I_h(z)$ of these reflections. Since the number L of such waves is rather small, this leads to a relatively simple dependence of the intensity of these reflections on the crystal thickness z. For example, when $L = 2$, which is often the case, this dependence is quasi-sinusoidal. In the reflections relating to the second group the excitation amplitudes $\omega^{j(L)}_{h(L+n)}$ $(n = 1, 2, ...)$ are comparable with the amplitudes $\omega^{L+n}_{h(L+n)}$ and are the first-order quantities [*cf.* (45), (46)]. This is the reason why the dependence $I_h(z)$ for the second group of reflections becomes more complicated. Moreover, the interaction of the free state $E^{L+n}_{\perp}$ with bound and valence states $E^{j(L)}_{\perp}$ decreases with increase in the number n and becomes comparable with the interaction with the nearest states $E^{L+n-1}_{\perp}$, $E^{L+n+1}_{\perp}$.

Table 1. *The parameters of multiwave diffraction for the problem shown in Fig.* 1 ($E = 75$ keV) (1 *analytical calculation*, 2 *computer calculations*)

$j(p)$		1(u)	2(B_1)	3(u)	4(B_1)	5(u)
$E^{j(p)}_{\perp}$ (eV)	1	−20·0	−2·8	23·1	34·2	64·7
	2	−21·2	−2·9	22·2	34·1	65·5
$\omega^{j(p)}_{020} \times 10$	1	4·18	4·96	0·776	0·030	0·028
	2	4·17	4·94	0·785	0·039	0·036

It is interesting to note that sometimes the curves $I_{h(L+n)}(z)$ have the same positions for the extrema as the kinematical curves. This is so because with a small number of bound states the levels $E^{j(L)}$ are not low-lying, as a rule, so that $|E^{j(L)}| \ll E^{L+n}$, and $E^{L+n} \simeq E^{L+n}_{\perp \text{kin}} = g^2(L+n) - V_0$. Several multiwave calculations for $I_h(z)$ at normal incidence were carried out by Vergasov, Chukhovskii & Pinsker (1985).

Here we represent the results for the calculations of the 020 reflection in the diffraction pattern shown in Fig. 1. As seen from the values of the multiwave diffraction parameters listed in Table 1, the highly excited waves for the 020 are three Bloch waves ($L = 3$): two Bloch waves (sub- and near-barrier ones) of the unitary representation, $L^{(u)} = 2$, and one near-barrier wave of the one-dimensional representation $D^{(B_1)}$. In this case the zeroth-order Bloch waves of the unitary representation $D^{(u)}$ are determined by the second-order dispersion equation corresponding to two stars labeled 1 and 2 in Fig. 1 and the zeroth-order near-barrier wave of the $D^{(B_1)}$ representation is obtained from the linear dispersion equation corresponding to star 1. In Fig. 2 the dependence $I_{020}(z)$ calculated analytically by means of these Bloch waves is shown. It is the sum of three cosinusoidal

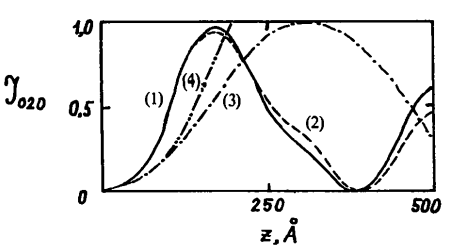

Fig. 2. The 020 reflection intensity $I_{020}(z)$ *versus* thickness z of the ⟨100⟩ LiF crystal in the case shown in Fig. 1. The electron energy $E = 75$ keV. Curves: (1) numerical calculation including 30 Bloch waves; (2) analytical calculation with three Bloch waves; (3) calculation within the two-beam (000, 020) approximation; (4) calculation within the kinematical approximation.

terms and is in good agreement with numerical calculations using 30 Bloch waves.

In regard to the formation of crystal lattice images in high-resolution electron microscopy (HREM) the intensity distribution in the image is given by

$$|\psi(\rho)|^2 = |\sum_j \psi_0^{j*}\psi^j(\rho)\exp(i2\pi k_{0z}^j z)|^2 \qquad (49)$$

neglecting the transfer function of an electron microscope.

In terms of the Bloch-wave distributions

$$\psi^j(\rho) = \sum_h \psi_h^j \exp(i2\pi h\rho) \qquad (50)$$

where $\rho = (x, y)$ is given in the image plane. Notice that under certain conditions HREM lattice images can be formed by a single Bloch wave (Kambe, 1982).

The relationship between the Bloch waves and the stars of the reciprocal-lattice vectors (27) permits us to determine *a priori* the main features of the electron wave function (50) in the unit cell and also to evaluate the penetration of these waves in the crystal. Since the strongest diffracted beams are close to the transmitted beam 000, the highly excited sub- and near-barrier wave functions are concentrated on atom rows. On one hand, this means that in the case of thin crystals these highly excited waves are localized on atomic sites, and the subsidiary maxima of $|\psi^{j(L)}(\rho)|^2$ do not correspond to positions of atoms.

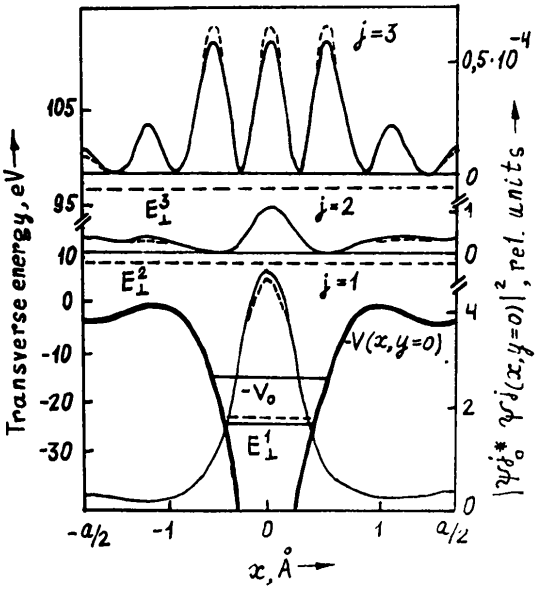

Fig. 3. Positions of levels of the transverse energy $E_\perp^j$ in the potential well $V(x, y = 0)$ and the distribution densities $|\psi_0^{j*}\psi^j(x, y = 0)|^2$ of the corresponding electron states in the unit cell of ⟨111⟩ Si at the electron energy $E = 100$ keV. The solid curves are the computed results and the broken lines are the analytical calculations.

On the other hand, it is just this circumstance that accounts for the stronger absorption of these waves compared with those above the barrier. The latter correspond to the stars of the weak reflections with large magnitudes for the reciprocal-lattice vectors and, therefore, their spatial densities oscillate. Nevertheless, since the above-barrier waves are not so highly excited as the sub- and near-barrier waves, atomic identification is feasible. At the same time, owing to their greater penetrating power, the above-barrier waves dominate starting from a certain crystal thickness and HREM lattice images become complicated. The above results are illustrated in Fig. 3.

6. Bloch waves in an imperfect crystal with point defects

For an imperfect crystal it is assumed that the lattice potential $V(r)$ can be represented as a sum of two components

$$V(r) = V(\rho) + W(\rho, z) \qquad (51)$$

where the term $W(\rho, z)$ corresponds to the deviation of the real potential from the z-averaged potential $V(\rho)$ of a perfect crystal.

In this case the wave function will be expressed as a series of Bloch waves

$$\psi(r) = \sum_j \alpha^j(r)\psi^j(\rho)\exp(2\pi i k_{0z}^j z), \qquad (52)$$

where the jth amplitudes $\psi^j(\rho)$ obey the equation

$$\Delta_\rho\psi^j(\rho) + 4\pi^2[K_0^2 - (k_{0z}^j)^2 + V(\rho)]\psi^j(\rho) = 0. \qquad (53)$$

Substitution of the wave function (52) into the Schrödinger equation (1) yields, in view of (53),

$$\sum_j [i4\pi k_{0z}^j \psi^j(\rho)\nabla_z\alpha^j(r) + 2\nabla_\rho\alpha^j(r)\nabla_\rho\psi^j(\rho) + \psi^j(\rho)\Delta_\rho\alpha^j(r) + \psi^j(\rho)\Delta_z\alpha^j(r) + 4\pi^2 W(r)\alpha^j(r)\psi^j(\rho)]\exp(2\pi i k_{0z}^j z) = 0. \qquad (54)$$

If κ is the characteristic length of variation for the function $\alpha^j(r)$ and G is the characteristic magnitude of the receiprocal-lattice vectors involved, we can easily obtain the following ratios of the first four terms contained in brackets on the left-hand side of (54):

$$4\pi k_{0z}^j : 4\pi G : \kappa^{-1} : \kappa^{-1}. \qquad (55)$$

For fast electrons we have

$$G/k_{0z}^j \le 1, \quad \kappa^{-1} \gtrsim G. \qquad (56)$$

Next, we represent the unknown function $\alpha^j(r)$ to first order by

$$\alpha^j \simeq {}_0\alpha^j + {}_1\alpha^j, \quad {}_0\alpha^j = \psi_0^{j*}, \qquad (57)$$

where the ${}_1\alpha^j$ values are assumed to be of the same order as W.

Substituting the expression (57) into (54) and taking into account the inequalities (56) we find to first order

$$\sum_j \psi^j(\rho)\exp(2\pi i k^j_{0z} z)\{ik^j_{0z}\partial[{}_1\alpha(r)]/\partial z + \pi W(r)\} = 0. \quad (58)$$

The orthonormalization property of the functions $\psi^j(\rho)$ within every nth unit cell yields

$$\int_\Omega \psi^{j*}(\rho_n + \rho)\psi^i(\rho_n + \rho)\mathrm{d}\rho = \delta_{ji},$$

where ρ_n is the radius vector of the nth unit cell in the plane (x,y). We then obtain the first-order solution of (58) in the form

$${}_1\alpha(z - z_0, \rho_n - \rho_0) = i\pi(k^j_{0z})^{-1}\int W^{ji}(z - z_0, \rho_n - \rho_0) \times \exp[2\pi i(k^j_{0z} - k^j_{0z})z]\mathrm{d}z, \quad (59)$$

where

$$W^{ji}(z - z_0, \rho_n - \rho_0) = \int_\Omega \psi^{j*}(\rho_n + \rho - \rho_0)W(\rho_n + \rho - \rho_0, z - z_0) \times \psi^i(\rho_n + \rho - \rho_0)\mathrm{d}\rho, \quad (60)$$

and $r_0 = (\rho_0, z_0)$ is the radius vector of a point defect located in the unit cell with $n = 1$.

The formulae (52), (57), (59), (60) yield the first-order solution of the problem of scattering of Bloch waves by the crystal lattice with point defects and represent the generalization of the solutions obtained by Indenbom, Tochilin & Chukhovskii (1988) on the basis of channeling theory. Unlike the case of a perfect crystal, now the excitation of Bloch waves, in the non-unitary irreducible representation of the symmetry group, occurs even under the condition of normal incidence. Equation (60) enables us to find the selection rules for exciting new Bloch waves in a crystal depending on the type of defects and, in principle, to elucidate the role of these Bloch waves for detecting point defects on a HREM image.

7. Electron-optical formulation of the multiwave diffraction theory

The electron-optical formulation of the multiwave diffraction theory elaborated originally by Cowley & Moodie (1959) is widely used for numerical calculations of HREM lattice images. Here we shall give the derivation of the main equations of the Cowley–Moodie theory starting from the Schrödinger equation in the integral form (Ishizuka & Uyeda, 1977; Danishevskii & Chukhovskii, 1982)

$$\psi(\mathbf{r}) = \exp(i2\pi\mathbf{K}_0\cdot\mathbf{r}) + \pi\int \mathrm{d}\mathbf{r}'\psi(\mathbf{r}')V(\mathbf{r}') \times \exp(i2\pi K_0|\mathbf{r} - \mathbf{r}'|)/|\mathbf{r} - \mathbf{r}'|. \quad (61)$$

Substituting the wave function $\psi(\mathbf{r}) = \exp(i2\pi\mathbf{K}_0\cdot\mathbf{r})\varphi(\mathbf{r})$ into (61) and using the parabolic approximation of Green's function $G(\rho,z) = (i\lambda z)^{-1}\exp(i\pi\rho^2/\lambda z)$ we obtain for the unknown function $\varphi(\mathbf{r})$ the Volterra integral equation of the second kind.

$$\varphi(\rho, z) = \int \mathrm{d}\rho'\varphi(\rho', z_0)G(\rho - \rho', z - z_0) + i\pi\lambda\int_{z_0}^{z}\mathrm{d}z'\int\mathrm{d}\rho'\varphi(\rho', z') \times V(\rho', z')G(\rho - \rho', z - z'). \quad (62)$$

Equation (62) is a convenient form for numerical calculations of the electron wave function $\varphi(\rho, z)$. In practice, however, the Cowley–Moodie equation

$$\varphi(\rho, z) = \int \mathrm{d}\rho'\varphi(\rho', z_0)\exp\{i\pi\lambda\int_{z_0}^{z}\mathrm{d}z'V(\rho, z')\} \times G(\rho - \rho', z - z_0) \quad (63)$$

is utilized. It is based on the electron-optical analog of electron diffraction in a crystal and follows from (62) if one assumes

$$\varphi(\rho', z') \simeq \varphi(\rho', z_0),$$
$$G(\rho - \rho', z - z') \simeq G(\rho - \rho', z - z_0),$$
$$1 + i\pi\lambda\int_{z_0}^{z}\mathrm{d}z'V(\rho', z') \simeq \exp[i\pi\lambda\int_{z_0}^{z}V(\rho, z')\mathrm{d}z']. \quad (64)$$

The approximations (64) are justified when the inequalities

$$\rho_{\mathrm{eff}} < z - z_0 < \rho^2_{\mathrm{eff}}2\pi\lambda^{-1} \quad (z - z_0 > 0)$$

are satisfied, where ρ_{eff} is the characteristic transverse length of variation of the potential function $V(\rho, z)$.

In order to calculate HREM lattice images it is convenient to make use of the recurrent relations between the Fourier components $\psi_n(hk)$, for the nth elementary layer in a crystal.

$$\psi(hk, z_n) \equiv \mathcal{F}\{\varphi(\rho, z_n); hk\} = S^{-1}\int \mathrm{d}\varphi(\rho, z_n) \times \exp\{-i2\pi\boldsymbol{\rho}.(h\mathbf{a}^{(*)} + k\mathbf{b}^{(*)})\}, \quad (65)$$

where $S = |\mathbf{a}\times\mathbf{b}|$ is the area of the unit cell on a plane perpendicular to the z axis; $\mathbf{a}^{(*)}$, $\mathbf{b}^{(*)}$ are the reciprocal-cell vectors corresponding to the unit-cell vectors $\mathbf{a}$, $\mathbf{b}$ of the crystal lattice.

As a result, from (63), we obtain

$$\psi_0(hk) = \delta_{h_0k_0},$$
$$\psi_{n+1}(hk) = \psi_n(hk)p_{n+1}(hk) * q_{n+1}(hk) \quad (66)$$

(the symbol $*$ means summation–convolution). Here the function $q_{n+1}(hk)$ is the Fourier transform of the phase function for the electron traversing a crystal of thickness $\Delta z_{n+1} = z_{n+1} - z_n$:

$$q_{n+1}(hk) = \mathcal{F}\left\{\exp\left[i\pi\lambda\int_{z_n}^{z_{n+1}}\mathrm{d}zV(\rho, z)\right]; hk\right\}. \quad (67)$$

The function $p_{n+1}(hk)$ is the Fourier transform of the electron propagation function in vacuum

$$p_{n+1}(hk) = S^{-1}\mathcal{F}\{G(\rho, z_{n+1} - z_n); hk\} = \exp(i2\pi\Delta z_{n+1} s_{hk}) \quad (68)$$

where s_{hk} is the excitation error of the reflection $hk0$.

Equations (66)–(68) describe the layer-to-layer calculation of the amplitudes $\psi_n(hk)$ (the so-called multislice method).

HREM lattice images are described by the contrast function

$$I(\rho) = \left| \sum_{h \in A} \psi(hk) \exp[ih\rho + i\chi(h)] \right|^2 \quad (69)$$

where the electron-optical phase function $\chi(h)$ is

$$\chi(h) = -\pi\lambda\Delta f h^2 + 2^{-1}\pi\lambda^3 C_s h^4 \quad (70)$$

where Δf is the defocusing parameter and C_s is the spherical aberration coefficient. The summation in (69) is over the diffracted beams passing through the aperture of the objective lens with size A. As follows from (69), the contrast function $I(\rho)$ is essentially determined by the defocusing parameter Δf and by the shape and size of the aperture A. Using ring apertures, for example, one can form 'fragment' images caused by reflections belonging to the star of equivalent nodes in the reciprocal lattice. These images will not depend on the electron-optical properties of the microscope and will be determined by the crystallographic function

$$\alpha_s(x, y) = \sum_{h_s, k_s} \cos[2\pi(h_s x + k_s y)], \quad (71)$$

where h_s, k_s are Miller indices of the reflections belonging to the sth star; x, y are the dimensionless coordinates in the unit cell of the crystal.

In the derivation of (71) we assumed that the stars consist of an even number of nodes. If, in addition, the main contribution to the image is provided by the reflections belonging to the first star, plus the central node, the contrast function (69) can be written as

$$I(\rho) = |\psi(0)|^2 + |\psi(h_1)|^2\alpha_1^2(\rho) + 2|\psi(0)||\psi(h_1)|\alpha_1(\rho) \times \cos\{\Gamma(h_1) + \chi(h_1)\}, \quad (72)$$

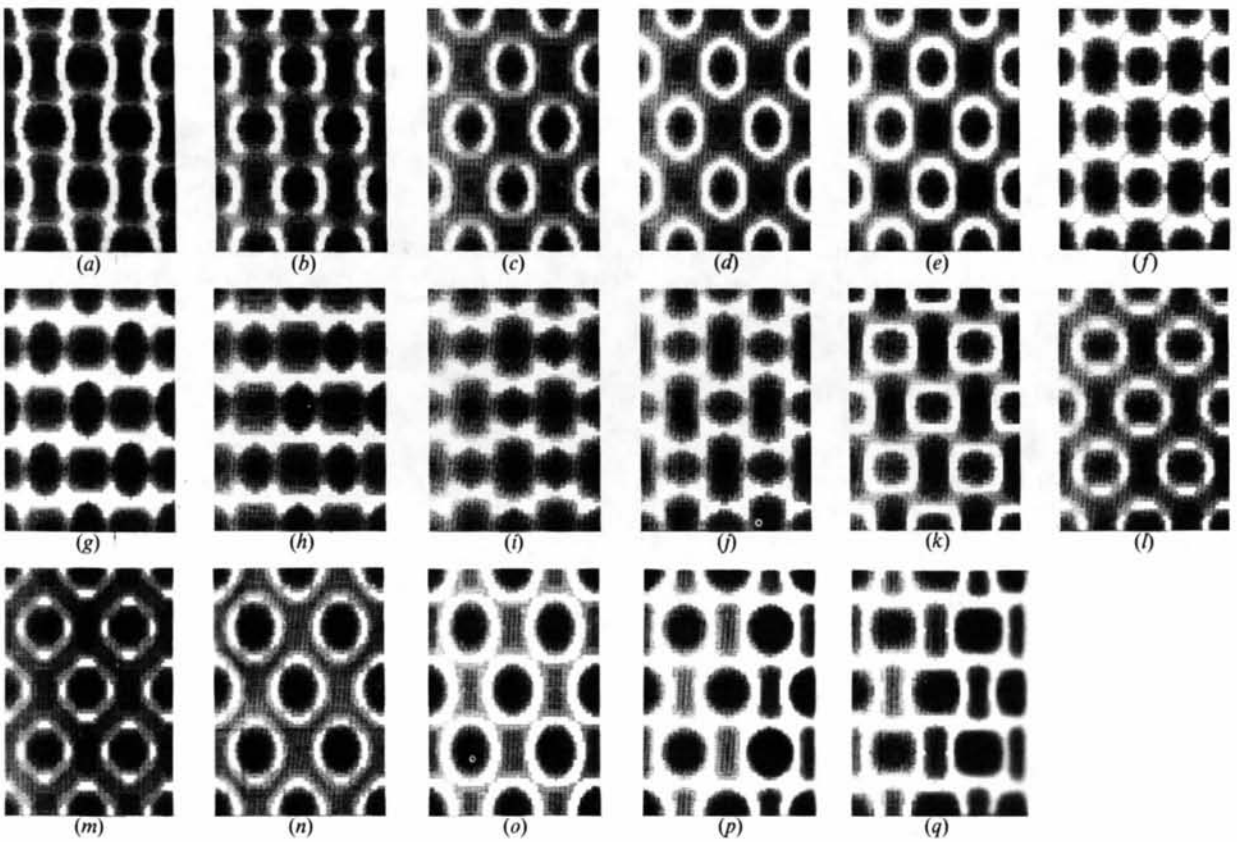

Fig. 4. Computer-simulated transmission images of the ⟨110⟩ Au crystal lattice. The film thickness is 40 unit cells (120 Å), $C_s = 1{\cdot}8$ mm, Δf varied from -200 to 200 Å with a step of 25 Å. 17 diffracted beams were included and the lattice spacing along ⟨110⟩ was divided into six layers. 2×2 unit cells.

where the relative phase of the diffracted beam h is equal to

$$\Gamma(h) = \mathrm{Im}\{\ln\psi(h) - \ln\psi(0)\}. \quad (73)$$

The contrast function (72) varies periodically with Δf, the period being equal to

$$\Delta f_p = 2/\lambda h_1^2. \quad (74)$$

It also follows from (72) that the contrast function $I(x, y)$ has extrema at the points (x, y) determined by the relations

$$\partial\alpha_1(x, y)/\partial x = 0, \quad \partial\alpha_1(x, y)/\partial y = 0. \quad (75)$$

As seen from (75), the extremum positions do not depend on the electron-optical phase function (70).

The condition of highest contrast is realized if the equality

$$\cos[\Gamma(h_1) + \chi(h_1)] = \pm 1 \quad (76)$$

holds. The quasi-kinematical scattering, when the diffracted beam amplitudes are small,

$$|\psi(h)| \begin{cases} \ll 1, & h \neq 0 \\ \simeq 1, & h = 0, \end{cases}$$

is physically of interest, and the contrast function $I(\rho)$ is a linearized function of the amplitudes $\psi(h)$

$$I(\rho) \simeq 1 + 2\sum_h |\psi(h)|\cos[2\pi h\rho + \Gamma(h) + \chi(h)]. \quad (77)$$

The expression (77) can be viewed as a hologram of the crystal lattice owing to the interference of the diffracted waves with the reference wave, the accuracy being controlled by the electron-optical phase $\chi(h)$.

It is interesting that in this case the expression (77) can be used to solve the inverse problem of diffraction – the reconstruction of the scattering function of an object

$$\varphi(\rho) = \sum_h \psi(h)\exp(i2\pi h\rho).$$

This method makes use of two-dimensional Fourier transforms $I_{\Delta f_m}(h)$ obtained in experiments at different Δf_m values ($m = 1, 2, \ldots$). It was applied in the famous work by Kirkland, Siegel, Uyeda & Fujioshi (1980).

In the general case, when the linearized approximation (77) is not applicable, computer simulations based on formulas (66)–(70) are used in order to study the formation of HREM images and to compare them with experiment.

As an example, we present here the results of computer simulations of the crystal lattice images of Au and Al–Y garnet. The atomic scattering amplitudes were calculated by the Doyle & Turner (1968) method. In order to draw simulated images a ten-point scale of $\ln(I_{\max}/I_{\min})$ within the unit-cell base was used.

In Fig. 4 the ⟨110⟩ Au lattice images are shown. In accordance with conditions (75) the coordinates of the extrema of the contrast function (72) are equal to

$$\begin{Bmatrix} x_0 \\ y_0 \end{Bmatrix} = \begin{Bmatrix} 0 & \frac{1}{4} & \frac{1}{2} & \frac{3}{4} \\ \frac{1}{4} & 0 & \frac{3}{4} & \frac{1}{2} \end{Bmatrix}$$

and form the sets of points

$$\begin{Bmatrix} x_0 \\ y_0 \end{Bmatrix} = \begin{Bmatrix} 0 & \frac{1}{2} \\ 0 & \frac{1}{2} \end{Bmatrix}, \quad \begin{Bmatrix} x_0 \\ y_0 \end{Bmatrix} = \begin{Bmatrix} 0 & \frac{1}{2} \\ \frac{1}{2} & 0 \end{Bmatrix},$$

the first (second) of which corresponds to maxima and minima of $I(\rho)$ at $\cos(\Gamma + \chi) = \pm 1$ [$\cos(\Gamma + \chi) = \mp 1$]. The defocusing period Δf_p (74) is equal to 300 Å and is in good agreement with the contrast variation of images calculated numerically (see Fig. 4). It is also seen that at certain Δf values the Au-atom images are surrounded by 'halos'. This effect is observed when the interference of the diffracted beams belonging to different stars is taken into account and it is not observed when only the reflections belonging to the first star are taken into account.

Fig. 5 shows the ⟨111⟩ $Y_3Al_5O_{12}$ crystal lattice images. As follows from calculations, the contribution to the image is provided mostly by the yttrium atoms. The projections of the yttrium atoms on the unit-cell base form two types of groups such as 'hexads' and 'triads' and have six- and threefold axes of symmetry, respectively (see Fig. 6). In the calculations the unit cell was divided into 24 layers; the calculation was carried out including 121 diffracted beams, *i.e.* the radius of the aperture was 0·4 $Å^{-1}$.

The 'hexads' and 'triads' of atoms are easily recognizable in Fig. 5. The spacing between hexad images

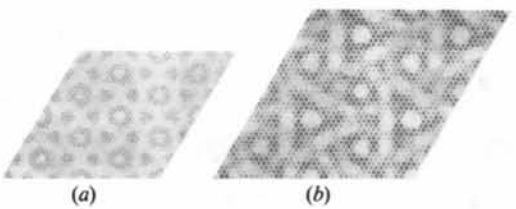

(*a*) (*b*)

Fig. 5. Computer-simulated images of ⟨111⟩ Al–Y garnet; C_s = 1·8 mm, 121 diffracted beams. (*a*) The film thickness is $3\frac{1}{12}$ of the crystal spacing (30 Å), $f = -800$ Å; (*b*) the film thickness is 1·25 of the crystal spacing (13 Å), $f = -900$ Å. 2 × 2 unit cells.

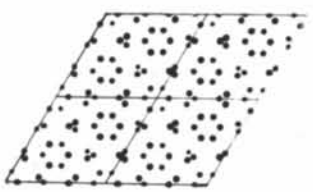

Fig. 6. Projections of the Y atoms on the base of the unit cell of Al–Y garnet. 2 × 2 unit cells.

is 10 Å and that between triad images is 17 Å, which correspond to the distances between the projections of the corresponding groups of atoms. The images with the threefold axis of symmetry are obtained when the atoms located at different heights provide essentially different contributions to the scattering. For example, when the thickness of the crystal object is 1·25 times as large as the lattice spacing along ⟨111⟩, the beam passes twice through the atoms located at heights $\frac{1}{12}$ and $\frac{3}{12}$, and through the others only once.

The authors thank A. L. Danishevskii for his assistance in the computer simulations.

References

BETHE, H. A. (1928). *Ann. Phys. (Leipzig)*, **87**, 55–129.

COWLEY, J. M. & MOODIE, A. F. (1959). *Acta Cryst.* **12**, 360–367.

DANISHEVSKII, A. L. & CHUKHOVSKII, F. N. (1982). *Kristallografiya*, **27**, 668–674.

DOYLE, P. A. & TURNER, P. S. (1968). *Acta Cryst.* A**24**, 390–398.

HIRSCH, P. B., HOWIE, A., NICHOLSON, B. B., PASHLEY, D. W. & WHELAN, M. J. (1965). *Electron Microscopy of Thin Crystals*. London: Butterworths.

HOWIE, A. & WHELAN, M. J. (1961). *Proc. R. Soc. London Ser. A*, **263**, 217–237.

INDENBOM, V. L., TOCHILIN, S. B. & CHUKHOVSKII, F. N. (1988). *Metallofizika*, **10**, 31–37.

ISHIZUKA, H. & UYEDA, N. (1977). *Acta Cryst.* A**33**, 740–749.

KALASHNIKOV, N. P., REMIZOVICH, V. S. & RYAZANOV, M. I. (1980). *Collisions of Fast Charged Particles in Solids*. Moscow: Atomizdat. (In Russian.)

KAMBE, K. (1982). *Ultramicroscopy*, **10**, 223–228.

KAMBE, K., FUJIMOTO, F. & LEHMPFUHL, G. (1974). *Z. Naturforsch. Teil A*, **29**, 1034–1044.

KIRKLAND, E. J., SIEGEL, B. M., UYEDA, N. & FUJIOSHI, Y. (1980). *Ultramicroscopy*, **5**, 479–503.

KOGISO, M. & TAKAHASHI, H. J. (1977). *J. Phys. Soc. Jpn*, **42**, 223–228.

KOMAKI, K., ASANO, S. & FUJIMOTO, F. (1977). Proc. Fifth Int. Conf. on High-Voltage Electron Microscopy, pp. 277–280. Kyoto, Japan.

LANDAU, L. D. & LIFSHITS, E. M. (1974). *Quantum Mechanics*. Moscow: Nauka. (In Russian.)

STEEDS, J. W., JONES, P. M., COOKE, K. & LOVELUCK, J. E. (1977). *Philos. Mag.* A**36**, 309–322.

STREITWOLF, H. (1967). *Gruppentheorie in der Festkörperphysik*. Leipzig: Akademische Verlagsgesellschaft.

VERGASOV, V. L. & CHUKHOVSKII, F. N. (1983). *Izv. Akad. Nauk SSSR Ser. Fiz.* **47**, 1174–1182.

VERGASOV, V. L., CHUKHOVSKII, F. N. & PINSKER, Z. G. (1982). *Kristallografiya*, **27**, 645–651.

VERGASOV, V. L., CHUKHOVSKII, F. N. & PINSKER, Z. G. (1984). *Dokl. Akad. Nauk SSSR*, **275**, 868–872.

VERGASOV, V. L., CHUKHOVSKII, F. N. & PINSKER, Z. G. (1985). *Kristallografiya*, **30**, 27–37.

VOROBIEV, S. A. (1984). *Channeling of Electron Beams*. Moscow: Energoizdat. (In Russian.)

Acta Cryst. (1990). A**46**, 165–170

An Accurate Reappraisal of the Elemental Form Factors and Charge Density of Copper

BY M. A. TABBERNOR

School of Construction, Engineering and Technology, The Polytechnic, Wulfruna Street, Wolverhampton WV1 1SB, England

AND A. G. FOX* AND R. M. FISHER

Center for Advanced Materials, Lawrence Berkeley Laboratory, University of California, Berkeley, California 94720, USA

(*Received* 23 *September* 1988; *accepted* 26 *September* 1989)

Abstract

The best X-ray atomic scattering factors for copper have been examined carefully to see which are most appropriate for charge density studies. The most consistent values were then used to generate a deformation charge density map, and it would appear that bonding in copper arises from electron charge build up between nearest-neighbour (n.n.) atoms, next-n.n. atoms *etc.* This is in agreement with conclusions obtained from γ-ray diffraction experiments and the best band-structure calculations, but in marked disagreement with the charge density obtained from earlier band-structure form factors.

Introduction

In most cases the differences between elemental X-ray atomic scattering factors and best free-atom values

* Present address: Department of Mechanical Engineering, Naval Postgraduate School, Monterey, CA 93943-5100, USA.

0108-7673/90/030165-06$03.00